

# High-resolution depth imaging with sparseness-constrained inversion

Jianfeng Zhang<sup>1,2</sup> and Kees Wapenaar<sup>1\*</sup>

<sup>1</sup>Department of Geotechnology, Delft University of Technology, PO Box 5028, 2600 GA Delft, the Netherlands, <sup>2</sup>Institute of Geology and Geophysics, Chinese Academy of Sciences, Beijing 100029, China

Received November 2004, revision accepted July 2005

## ABSTRACT

An imaging technique is developed which exceeds the resolution limitation prescribed by conventional seismic imaging methods. The high-resolution imaging is obtained by introducing a sparseness-constrained least-squares inversion into the imaging process of prestack depth migration. This is implemented by a proposed interference technique. In contrast to conventional depth migration, a decomposed signal or combined event, instead of the source wavelet, is needed in the proposed scheme. The proposed method aims to image a small local region with a higher resolution using the prestack data set. It should be applied following conventional depth imaging if a higher resolution is needed in a target zone rather than replacing the conventional depth imaging for the entire medium. Synthetic examples demonstrate the significant improvements in the resolution using the proposed scheme.

## INTRODUCTION

Some reservoirs consist of stacked sheet sands, the thickness of which is frequently less than one-quarter of the available seismic wavelength. A high-resolution imaging scheme is therefore important in order to improve understanding of these reservoirs and to optimize well placement. Deconvolution (Robinson 1967; Claerbout 1976) is the first approach to improving the resolution of seismic imaging. However, the usual assumptions about the wavelet phase and the statistics of the reflectivity restrict its applications in prestack imaging. Theoretically, non-linear inversion schemes based on optimal-fit-in-data-space (e.g. Jin *et al.* 1992) can achieve a high-resolution imaging beyond the limitation of the scale of the seismic wavelength. However, the computational cost of this type of method is too high for it to be applied to complicated structures, and the local minima and ill-posed problems require further study. Deconvolution and non-linear inversion methods are two of the usual approaches to improving the resolution of seismic imaging by extending the frequency-band of seismic signals and by imaging using multiple reflected waves. The former operation is usually carried out in deconvolution

using the prewhitening technique (Claerbout 1976). Other more effective but more expensive algorithms for extending the frequency-band of seismic signals have also been proposed, including linear programming reconstruction (Levy and Fullagar 1981; Oldenburg, Scheuer and Levy 1983), autoregressive modelling (Walker and Ulrych 1983), and minimum entropy reconstruction (Sacchi, Velis and Cominquez 1994). On the other hand, we aim to improve the resolution by extending the frequency-band of the resulting reflection coefficients.

In contrast to time migration, prestack depth migration can put each event at its true location, even in a strong laterally varying medium. Since the sharper focusing of reflected energy is essential for high-resolution imaging in a complicated subsurface, we prefer to follow the prestack depth-imaging approach in order to improve the resolution. Instead of increasing the available frequency-band of the seismic signal, as is done in conventional high-resolution seismic methods, we improve the resolution by introducing a new concept to the imaging algorithm. As is known, prestack depth migration is accomplished by combining wavefield extrapolation with the imaging condition. The downward wavefield extrapolation aims to remove the propagation effects of the overburden between the recording surface and each subsurface reflector, using one-way propagators. This is crucial for putting each event at its true location with focusing of reflected energy, and

---

\*E-mail: C.P.A.Wapenaar@citg.tudelft.nl  
zhangjf@mail.igcas.ac.cn

it is also important for improving the resolution. Moreover, the different imaging conditions also have different effects on the resolution of the imaging. The correlation condition (Claerbout 1971) produces wavelet stretch that degrades the resolution, whereas the deconvolution imaging condition (Claerbout 1976; Berkhout 1982) yields a band-limited reflection coefficient at each subsurface reflector by removing the effect of the wavelet. However, the latter is implemented only if the source wavelet has been exactly estimated. Due to the two facts that (a) the exact source wavelet is not easily obtained and (b) the wavelet exhibits variations along the propagation path in the presence of (intrinsic) attenuation, a scheme that improves the resolution without using the source wavelet will be more useful.

Sparse inversion, as proposed by Sacchi and Ulrych (1996), can produce a mode that consists of the minimum number of events that can satisfy the data by introducing Cauchy regularization. This linear inversion method has been widely applied to seismic signal processing, for example, in the Radon transform (Trad, Ulrych and Sacchi 2003), in the discrete Fourier transform (Sacchi and Ulrych 1996) and in seismic wave reconstruction (Wang 2003). Since a sparse solution in the time domain means a wider frequency-band, this method can also serve as a tool to extend the frequency-band of the resulting reflection coefficients. However, incorporating the sparse inversion with prestack depth migration is not straightforward. Following optical interferometry (Welford 1981), we have developed an interference technique to transform the imaging of reflection coefficients into a least-squares inversion without the source wavelet. Thus, a sparseness constraint can be easily introduced into the imaging of reflection coefficients by solving this linear inversion problem with Cauchy regularization. As a result, the frequency-band of the resulting reflection coefficients is extended and a higher-resolution imaging is obtained. This approach represents an alternative imaging algorithm in prestack depth migration. In contrast, the migration deconvolution (Hu, Schuster and Valasek 2001) improved the resolution by eliminating the acquisition footprint due to a spatially undersampled and limited aperture, but remained in the frequency-band of the reflection coefficients.

In order to reduce the computational cost and also to obtain a more stabilized solution of the inverse problem, we retain only the reflection events resulting from the target zone of interest, and try to mute other events before using the interference technique. The number of unknown reflection coefficients is thus considerably reduced and the solution of the related inverse problem becomes easier. Hence, the proposed scheme is suited to imaging a small local region with

a higher resolution, rather than replacing the conventional depth-imaging schemes for the entire medium.

The proposed sparse inversion, together with the interference technique, is applied to half-migrated data. It can also be employed to improve the resolution in full-migrated data, and even poststack data, provided that the wavelet remains stationary and both the reflected and diffracted energy are put at their true locations in the related data sets. The reason for using the half-migrated data here is because the wavelet remains perfectly stationary in this data space when expressed in the traveltime from the source to the subsurface reflectors (assuming attenuation can be neglected).

The paper is organized as follows. Firstly, prestack depth migration is very briefly reviewed and a half-migration technique is proposed to obtain a half-migrated shot gather expressed in the time domain. The interference technique is then proposed; this transforms the imaging process into a least-squares inversion. Next, a sparse solution for the reflection coefficients is discussed, and its numerical implementation is presented. After this, the depth mapping is briefly discussed. Finally, two synthetic seismic experiments are designed to test the proposed high-resolution imaging scheme.

## HALF-MIGRATION

Prestack depth migration is commonly accomplished by combining downward wavefield extrapolation, i.e. removing the propagation effects of the overburden between the recording surface and each subsurface reflector, with an imaging condition. If proper one-way propagators are used with a correct macro velocity model, prestack depth migration can put each event at its true location, even in a strong laterally varying medium. This is an important advantage of prestack depth migration in contrast to other imaging methods. If  $P^D(\mathbf{x}, \omega)$  denotes the forward extrapolated source wavefield and  $P^U(\mathbf{x}, \omega)$  denotes the inverse extrapolated shot gather in the space–frequency domain, the imaging can be obtained by two imaging conditions, i.e. the correlation imaging condition (Claerbout 1971), expressed as

$$\Phi_c(\mathbf{x}) = \int P^U(\mathbf{x}, \omega) \{P^D(\mathbf{x}, \omega)\}^* d\omega, \quad (1)$$

and the deconvolution imaging condition (Claerbout 1976; Berkhout 1982), given by

$$\Phi_d(\mathbf{x}) = \int \frac{P^U(\mathbf{x}, \omega) \{P^D(\mathbf{x}, \omega)\}^*}{P^D(\mathbf{x}, \omega) \{P^D(\mathbf{x}, \omega)\}^* + \varepsilon} d\omega, \quad (2)$$

where the superscript  $*$  denotes the complex conjugate,  $\varepsilon$  is a small stabilization constant,  $\mathbf{x} = (x, y, z)$  is the Cartesian

coordinate vector, and  $\omega$  is the angular frequency.  $\Phi_d(\mathbf{x})$  in (2) represents the band-limited reflection coefficients of the subsurface if the source wavelet used is exact. Unfortunately, the exact estimation of the source wavelet is not easy.

Since the wavelet exhibits space-variance resulting from varying velocities in an inhomogeneous medium but behaves time-invariant (assuming attenuation can be neglected), it will be more convenient to remove the effect of the source wavelet in the time domain, rather than in the depth domain. Therefore, a half-migration technique, which can obtain a half-migrated shot gather expressed in the time domain, is proposed, based on inverse wavefield extrapolation. If  $T(\mathbf{x})$  denotes the traveltimes for the source wavefield to arrive at each spatial gridpoint and  $A(\mathbf{x})$  denotes the corresponding amplitudes, obtained by solving the eikonal and transport equations (e.g. Buske and Kastner 2004), the half-migrated shot gather in the depth domain can be obtained as

$$\Phi(\mathbf{x}) = \int \frac{P^U(\mathbf{x}, \omega)}{A(\mathbf{x})} \exp\{j\omega T(\mathbf{x})\} d\omega, \quad (3)$$

where  $j$  is the imaginary unit. The term  $\exp\{j\omega T(\mathbf{x})\}$  in (3) applies a time-shift to the inverse extrapolated wavefield for compensating the traveltime from the source to the subsurface reflectors, and the frequency-independent amplitude  $A(\mathbf{x})$  compensates for the geometrical spreading of the source wavefield. Furthermore, we can obtain the half-migrated shot gather  $\Phi'(x, y, t)$ , expressed in the time domain, by replacing depth  $z$  with the related traveltime  $t = T(x, y, z)$  for each receiver position  $(x, y)$ . From the point of view of reciprocity, each trace in  $\Phi'(x, y, t)$  can be understood as a record that would be measured at the source position (in the time-domain) when all reflectors along the depth direction at the related receiver position simultaneously excited the same wavelet (without the geometrical spreading), as illustrated in Fig. 1. We therefore refer to this proposed migration scheme as ‘half-migration’. The high-resolution imaging scheme will be developed following the half-migrated result because it is natural to get a perfect stationary wavelet in this data space. There are two reasons for the half-migrated shot gather to be expressed in terms of the traveltime from the source to the subsurface reflectors rather than in the vertical traveltime. The first is that this traveltime has already been obtained in the half-migration process, so no additional calculation is required to obtain the traveltime of each subsurface point. The second is that the wavelet can remain stationary better in this time domain. This can be explained by assuming a homogeneous medium in Fig. 1. From the geometry shown in Fig. 1, we obtain

$$c\Delta T_v \approx c\Delta T \sin \theta + cT\Delta\theta \cos \theta, \quad (4)$$

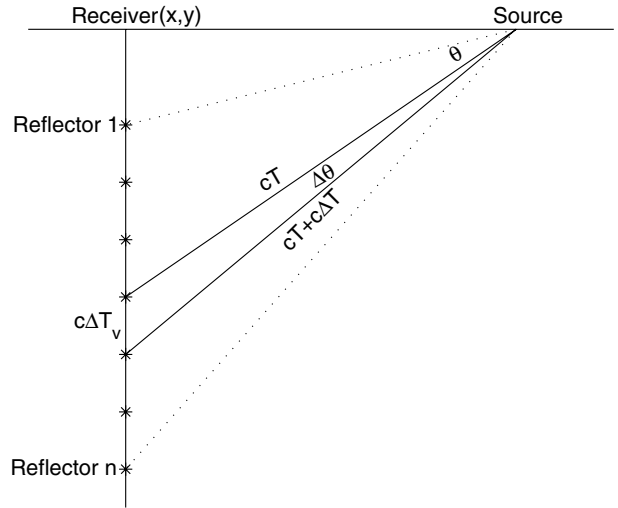


**Figure 1** Illustration of the half-migration technique. The half-migrated shot gather can be understood as a record that would be measured at the source position when reflectors 1, etc., along the depth direction simultaneously excite the same wavelet. The medium is assumed to be homogeneous so that the rays from the source to the subsurface reflectors are straight.  $c$  is the P-wave velocity,  $\Delta T$  is the true duration of the wavelet, and  $\Delta T_v$  is the duration of the wavelet when expressed in terms of the one-way vertical traveltime.

where  $c$  is the P-wave velocity and  $\Delta T$  is the true duration of the source wavelet. When the half-migrated result is expressed in terms of the one-way vertical traveltime, the duration of the wavelet is given by  $\Delta T_v$ , whereas the duration of the wavelet becomes  $\Delta T$  when the same half-migrated result is expressed in terms of the traveltime from the source to the subsurface reflectors, as illustrated in Fig. 1. We know from (4) that  $\Delta T_v$  exhibits slight variations for the reflectors at the different depths. In contrast, the duration of the wavelet in the proposed time domain (i.e. time from the source to the subsurface reflectors),  $\Delta T$ , remains stationary.

The proposed half-migration technique may encounter the multipath arrival problem in complex media as a result of using ray theory in the forward extrapolation of the source wavefield. Usually, this problem can be well handled by using the maximum energy arrival rather than the first arrival in the calculation of the traveltime. Alternatively, if the maximum energy scheme fails to obtain a desirable half-migrated result, we can obtain the half-migrated shot gather in the depth domain by replacing the source wavelet in (2) with an impulse at zero time. This means that we also calculate  $A(\mathbf{x}) \exp\{-j\omega T(\mathbf{x})\}$  using the wave-equation-based algorithm. However, an additional computation to get the (maximum energy) traveltime from the source to each point  $(x, y, z)$ , i.e.  $T(\mathbf{x})$ , is then

required for expressing the half-migrated shot gather in the time domain.

## INTERFERENCE TECHNIQUE

Provided that (intrinsic) attenuation is neglected, each trace in the half-migrated shot gather can be expressed in the frequency domain as

$$\hat{\Phi}'(x, y, \omega) = \sum_{i=1}^n r_i S(\omega) \exp(-j\omega t_i), \quad (5)$$

where  $S(\omega)$  is the spectrum of the source wavelet,  $t_i$  is the traveltime from the point at the horizontal position  $(x, y)$  at the  $i$ th reflector (along the depth direction, see Fig. 1) to the source position,  $r_i$  is the reflection coefficient at the related point of the  $i$ th reflector, and  $n$  is the total number of reflectors along the depth direction at the horizontal position  $(x, y)$ . If we further assume that all angles of incidence are less than the corresponding critical angles (which is a common assumption in seismic processing), all the reflection coefficients  $r_i$  will be real in (5). By following optical interferometry (Welford 1981), one of the arrivals, e.g.  $a_1(\omega) = r_1 S(\omega) \exp(-j\omega t_1)$ , is defined as the reference arrival. This reference arrival can be obtained by decomposing the corresponding trace using time–frequency spectral analysis (e.g. Pinnegar and Mansinha 2003) or by decomposing the related half-migrated shot gather using the generalized Randon transform (e.g. Trad *et al.* 2003). We then define the interference between the reference arrival and the related trace as follows:

$$j(\hat{\Phi}' \cdot a_1^* - \hat{\Phi}^* \cdot a_1) = 2a_1 a_1^* \sum_{i=2}^n (r_i/r_1) \sin[\omega(t_i - t_1)]. \quad (6)$$

Rewriting (6) as

$$\sum_{i=2}^n \bar{r}_i \sin[\omega(t_i - t_1)] = j(\hat{\Phi}' \cdot a_1^* - \hat{\Phi}^* \cdot a_1) / 2a_1 a_1^* = y(\omega), \quad (7)$$

where  $y(\omega)$  is a known real-valued function obtained from the half-migrated shot gather and  $\bar{r}_i = r_i/r_1$  is a relative reflection coefficient, we obtain a new equation for the reflection coefficients from the proposed interference technique. Instead of solving (7) by the discrete Fourier series (considering  $\omega$  as a variable), which will again produce band-limited reflection coefficients, a sparse inversion is introduced to solve (7). This sparse inversion represents an alternative imaging algorithm, in comparison with (1) or (2), used in conventional depth migration.

Note that it is not necessary for the reference arrival to be a reflection from a single reflector. A combined reflection, e.g. the reflection from a ‘thin bed’, can also serve as a reference

arrival. The reflection from a ‘thin bed’ is given by  $a_1(\omega) = r_1 j\omega \Delta t_1 S(\omega) \exp(-j\omega t_1)$ . Here  $\Delta t_1$  denotes the difference in the traveltime between the upper and lower surfaces of the ‘thin bed’. Taking this combined reflection as a reference arrival and defining a new formulation for the interference as in the following, we have

$$\hat{\Phi}' \cdot a_1^* + \hat{\Phi}^* \cdot a_1 = 2a_1 a_1^* \sum_{i=2}^n (r_i/r_1 \Delta t_i) \frac{1}{\omega} \sin[\omega(t_i - t_1)]. \quad (8)$$

This equation is similar to (7). If we further rewrite each trace in the half-migrated shot gather as a summation of the reflections from many ‘thin beds’ (which is true for some reservoirs that consist of stacked sheet sands), we obtain

$$\hat{\Phi}'(x, y, \omega) = \sum_{i=1}^n r_i \Delta t_i j\omega S(\omega) \exp(-j\omega t_i), \quad (9)$$

where  $\Delta t_i$  is determined by the thickness of each ‘thin bed’ and  $n$  is the number of ‘thin beds’ rather than that of the reflectors. Substituting the reference arrival of the reflection from a ‘thin bed’ and (9) into the left-hand side of (6) leads to

$$j(\hat{\Phi}' \cdot a_1^* - \hat{\Phi}^* \cdot a_1) = 2a_1 a_1^* \sum_{i=2}^n (r_i \Delta t_i / r_1 \Delta t_1) \sin[\omega(t_i - t_1)]. \quad (10)$$

We obtain an equation exactly the same as (7). Equations 8 and 10 demonstrate the flexibility of the choice of the reference arrival in the proposed interference technique. Equation (10) also means that we do not need to distinguish the upper and lower surfaces of each ‘thin bed’ in the imaging. This is very important when a ‘thin bed’ becomes too thin to be distinguished, even using the sparse inversion. Since (8) is similar to (7), and (10) is the same as (7) with  $\bar{r}_i = r_i \Delta t_i / r_1 \Delta t_1$ , we only discuss the solution of the sparse inversion of (7) in the following.

## SPARSE INVERSION

Define the real vector  $\mathbf{R}$  as the unknown reflection series with its  $m$ th component denoting the relative reflection coefficient at time  $t_1 + t_0 + m\Delta t$ . Here  $t_1$  is the traveltime of the reference arrival,  $t_0$  is the estimated smallest time difference between the reference arrival and other available arrivals, and  $m$  varies from 1 to  $N$ . The number  $N$  is determined by the estimated largest time difference between the reference arrival and other available arrivals.  $t_0$  is introduced to reduce the number of the unknown relative reflection coefficients. Equation (7) can then be rewritten as

$$\mathbf{G}\mathbf{R} = \mathbf{Y}, \quad (11)$$

where the component  $\{\mathbf{Y}\}_k$  of the real vector  $\mathbf{Y}$  is defined as  $y[\omega_{\min} + (k - 1)\Delta\omega]$ , and the element  $\{\mathbf{\Gamma}\}_{km}$  of the real matrix  $\mathbf{\Gamma}$  is defined as  $\sin\{[\omega_{\min} + (k - 1)\Delta\omega](t_0 + m\Delta t)\}$ . Here  $\omega_{\min}$  is the minimum frequency of the seismic signals, and  $k$  varies from 1 to  $M$  with  $M = \text{int}\{(\omega_{\max} - \omega_{\min})/\Delta\omega\}$  ( $\omega_{\max}$  is the maximum frequency of the seismic signals). In the following, all discussions on the reflection coefficients refer to the relative reflection coefficients expressed in (7). Except for the case  $N = M$ , equation (11) is either underdetermined or overdetermined. Therefore, the solution of (11) should be transformed into a least-squares problem expressed by

$$\min \{J(\mathbf{R}) = (\mathbf{R}^T \mathbf{\Gamma}^T - \mathbf{Y}^T) \mathbf{\Lambda}^T (\mathbf{\Gamma} \mathbf{R} - \mathbf{Y}) + \mathbf{R}^T \mathbf{W} \mathbf{R}\}, \quad (12)$$

where  $\mathbf{W}$  is a real-valued diagonal matrix whose elements are determined by the regularized mode for overcoming non-uniqueness of the solution, and  $\mathbf{\Lambda}$  is a real-valued diagonal matrix whose elements denote the weight factors for different frequencies. Here, the diagonal elements of  $\mathbf{\Lambda}$  are defined as  $\{\mathbf{\Lambda}\}_{kk} = \omega_{\min} + (k - 1)\Delta\omega$  for weighting the high-frequency components. The solution of (12) is obtained as

$$\mathbf{R} = (\mathbf{\Gamma}^T \mathbf{\Lambda}^T \mathbf{\Lambda} \mathbf{\Gamma} + \mathbf{W})^{-1} \mathbf{\Gamma}^T \mathbf{\Lambda}^T \mathbf{\Lambda} \mathbf{Y}. \quad (13)$$

It can be seen that (13) needs the inversion of an  $N \times N$  matrix. If  $N > M$ , using the identity,

$$(\mathbf{\Gamma}^T \mathbf{\Lambda}^T \mathbf{\Lambda} \mathbf{\Gamma} + \mathbf{W}) \mathbf{W}^{-1} \mathbf{\Gamma}^T \mathbf{\Lambda}^T \equiv \mathbf{\Gamma}^T \mathbf{\Lambda}^T (\mathbf{\Lambda} \mathbf{\Gamma} \mathbf{W}^{-1} \mathbf{\Gamma}^T \mathbf{\Lambda}^T + \mathbf{I}), \quad (14)$$

we can rewrite (13) as

$$\mathbf{R} = \mathbf{W}^{-1} \mathbf{\Gamma}^T \mathbf{\Lambda}^T (\mathbf{\Lambda} \mathbf{\Gamma} \mathbf{W}^{-1} \mathbf{\Gamma}^T \mathbf{\Lambda}^T + \mathbf{I})^{-1} \mathbf{\Lambda} \mathbf{Y}, \quad (15)$$

where  $\mathbf{I}$  is an  $M \times M$  identity matrix. Equation (15) requires the inversion of an  $M \times M$  matrix, instead of an  $N \times N$  matrix. The computational cost is therefore reduced for the situation  $N > M$ .

By setting  $\mathbf{W} = \mu \mathbf{I}$ , where  $\mu$  is a small positive constant, Gaussian regularization is imposed and a smoothed solution is obtained from either (13) or (15). This smoothed solution again represents band-limited reflection coefficients without a significant improvement in the resolution. If Cauchy regularization, as proposed by Sacchi and Ulrych (1996), is introduced to the least-squares problem, a sparse solution, i.e. the solution that is able to satisfy the data with the smallest number of reflection events, can be obtained from either (13) or (15). This sparse solution represents a higher-resolution result in the time domain. The related diagonal matrix  $\mathbf{W}$  defined by Cauchy regularization is therefore referred as the sparseness constraint.

The sparseness constraint matrix  $\mathbf{W}$  (diagonal matrix) is determined according to a priori information about the so-

lution, that is, the diagonal elements related to the reflection events should be small whereas the other diagonal elements will be large enough to suppress the appearance of significant values. The optimal choice for the sparseness constraint remains a topic of research. Sacchi and Ulrych (1996) suggested an iterative algorithm where  $\mathbf{W}$  is bootstrapped from the result of a previous iteration. Wang (2003) defined a sparseness constraint by taking the smoothed solution as a priori information following a similar formulation to that suggested by Sacchi and Ulrych (1996). Here, we also construct the sparseness constraint matrix according to the smoothed solution, obtained by setting  $\mathbf{W} = \mu \mathbf{I}$  in either (13) or (15). However, unlike Sacchi and Ulrych (1996) and Wang (2003), we allow the diagonal elements of  $\mathbf{W}$  to vary following an exponential function expressed as

$$\{\mathbf{W}\}_{mm} = \alpha_{\max} (\alpha_{\min}/\alpha_{\max})^{\frac{|r_m| - \beta_{\min}}{\beta_{\max} - \beta_{\min}}}, \quad (16)$$

where  $||$  denotes the modulus,  $r_m$  is  $m$ th component of the smoothed  $\mathbf{R}$ ,  $\beta_{\max} = \max\{|r_m|, m = 1, N\}$ ,  $\beta_{\min} = \min\{|r_m|, m = 1, N\}$ ,  $\alpha_{\max}$  is the prescribed maximum factor to suppress the appearance of unwanted reflections, and  $\alpha_{\min}$  is the prescribed minimum factor to boost the reflected events. Equation (16) means that the maximum smoothed solution is related to the minimum factor  $\alpha_{\min}$ , whereas the minimum smoothed solution is related to the maximum factor  $\alpha_{\max}$ . By using the sparseness constraint defined in (16), a desirable sparse solution can be obtained.

If some arrivals, which do not result from the target zone of interest, are muted in advance, the number of the unknown reflection coefficients, i.e.  $N$ , can be greatly reduced. As a result, the solution of (11) becomes easy and a more stabilized result can be obtained from either (13) or (15). Due to the small traveltimes differences between those arrivals included in (5) in this case, two additional benefits are also achieved. In particular the time-variance of the wavelet due to (intrinsic) attenuation can be neglected in (5), and the geometrical spreading factors, i.e. the amplitude  $A(\mathbf{x})$  used in (3), can be taken as a constant. Thus, the calculation of amplitudes by solving the transport equation can be omitted in the half-migration processing. We therefore prefer to obtain higher-resolution imaging in a local target zone of interest by following this muting processing. Many techniques, e.g. Radon transform and time-frequency spectral analysis, can be used to mute the events that are not of interest. It should be pointed out that the reference arrival does not need to be a reflection resulting from the target zone of interest. A time-shift technique can be used if the traveltime difference between the reference arrival and the reflection

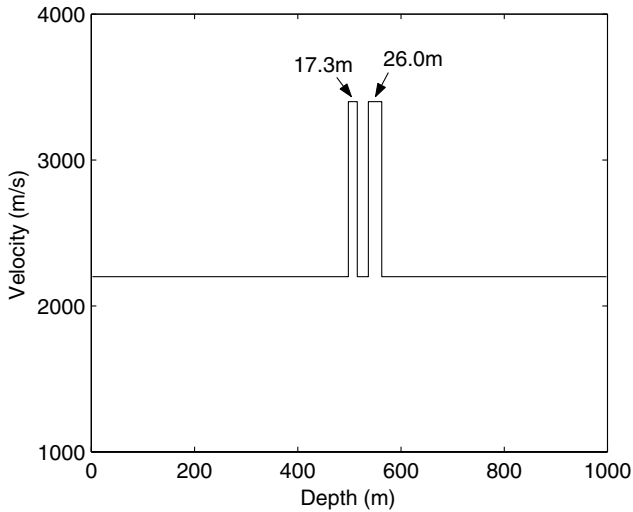


Figure 2 Vertical velocity profile in a laterally invariant model. The thicknesses of the high-velocity thin layers are 17.3 m and 26.0 m, respectively.

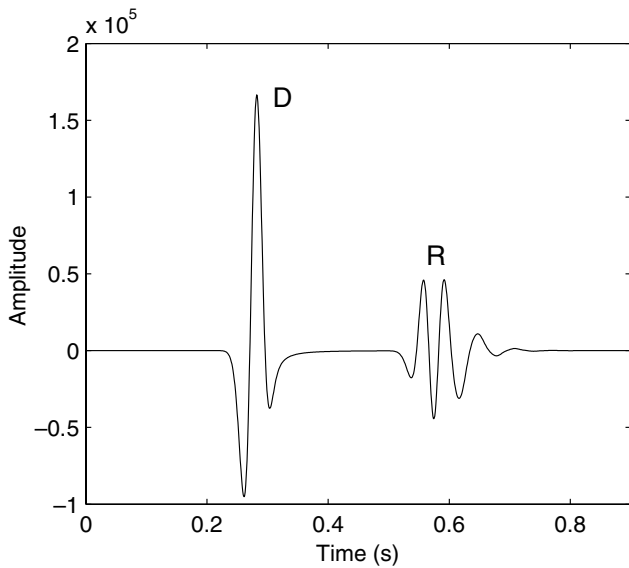


Figure 3 A trace of the shot record at offset 500 m. The direct wave (D) and the reflected waves as well as internal multiples (R) are all included.

events of interest is too large. Moreover, it is unnecessary for the reference arrival to be exactly a reflection from a single reflector (see discussion below (10)).

The proposed sparse inversion, together with the interference technique, is not confined only to the half-migrated data. It can serve as a tool to improve the resolution of full-migrated data, and even of poststack data, provided that the wavelet remains stationary. In contrast to other available sparse-spike

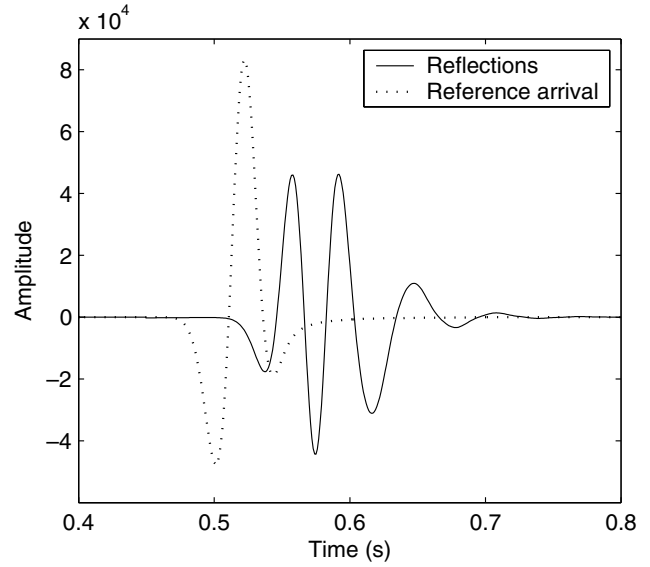


Figure 4 Reference arrival and reflections from the target zone. A time-shift and amplitude scaling have been applied to transform the direct wave into a reference arrival.

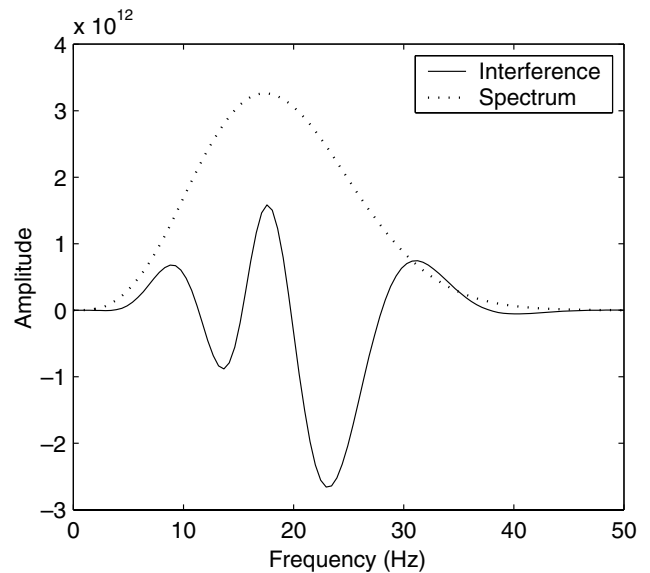
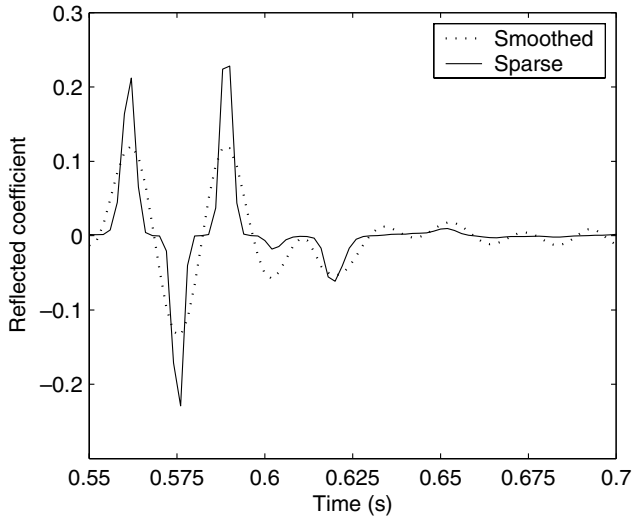
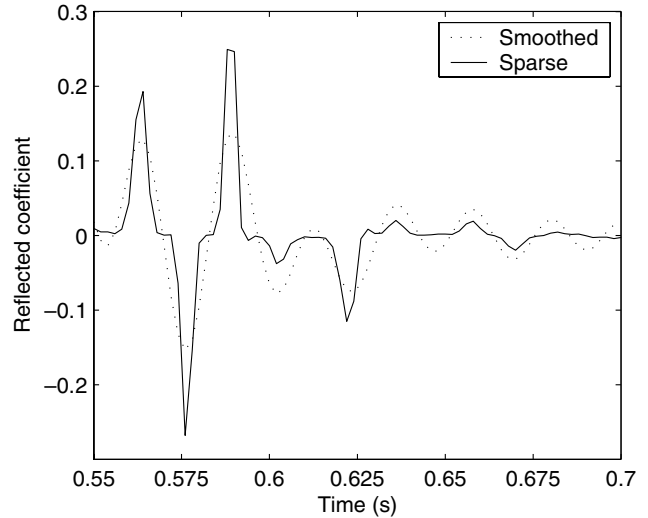


Figure 5 Result of the interference expressed in the frequency domain, showing the interference between the reference arrival and the reflections from the target zone, and the amplitude spectrum of the reference arrival.

inversion techniques (Levy and Fullagar 1981; Oldenburg *et al.* 1983; Sacchi *et al.* 1994), the proposed scheme requires an extraction of the reference arrival, instead of an appraisal deconvolution, to be applied in advance. Furthermore, the sparse-spike inversion schemes in Levy and Fullagar (1981), Oldenburg *et al.* (1983) and Sacchi *et al.* (1994) used the



**Figure 6** Comparison between the sparse and smoothed solutions. Note that in the sparse solution the four reflections from the closely spaced reflectors are well separated with correct polarity. The internal multiples included in the shot record explain the poor estimation of the magnitude of the 4th spike.



**Figure 8** Sparse and smoothed solutions for the noisy data. The same computational procedure as used to obtain the result of Figure 6 is applied. Note that a sparse solution similar to that in Figure 6, with the spikes in the same positions, is obtained in spite of the significant noise in the data.

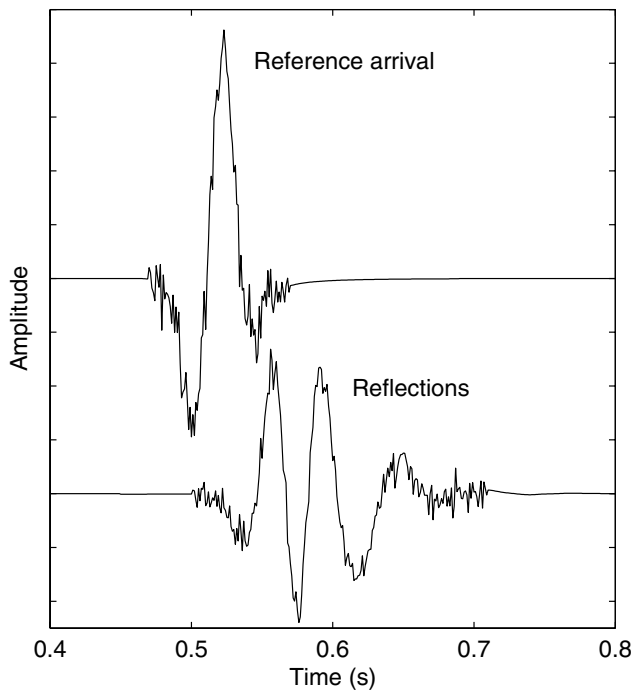


**Figure 7** Noisy reference arrival and reflection data. The display is obtained by adding white noise to both the reference arrival and the reflections from the target zone shown in Figure 4. The ratio of the rms of the noise to the maximum value of the signal is 0.08 for both the reference arrival and the reflection data.

limited frequency-band output of the appraisal deconvolution as the constraints of the optimization problem. The output of the appraisal deconvolution will therefore fully govern the final results of the sparse-spike inversion. That is, the errors in the output of the appraisal deconvolution will not be modified by the sparse-spike inversion techniques. Moreover, an iteration scheme has to be used for solving the resulting constrained (non-linear) optimization problems in the above-mentioned sparse-spike inversion techniques.

### NUMERICAL IMPLEMENTATION

The numerical implementation of the proposed sparse inversion, together with the interference technique, is illustrated with a synthetic shot record resulting from a model with two closely spaced thin layers. Due to the laterally homogeneous medium, the half-migration processing, which is similar to conventional prestack depth migration, is omitted. Figures 2 and 3 show a laterally invariant velocity model and a trace of the shot record at offset 500 m, respectively. A Ricker wavelet point source with a peak frequency of 20 Hz is used in generating the shot record. Both the direct and reflected (including internal multiples) waves are included in Fig. 3. For this particular case, the direct wave is taken as the reference arrival and the muting processing is easily accomplished by removing the direct wave, as illustrated in Fig. 4, where a time-shift and amplitude scaling have been applied to the reference arrival

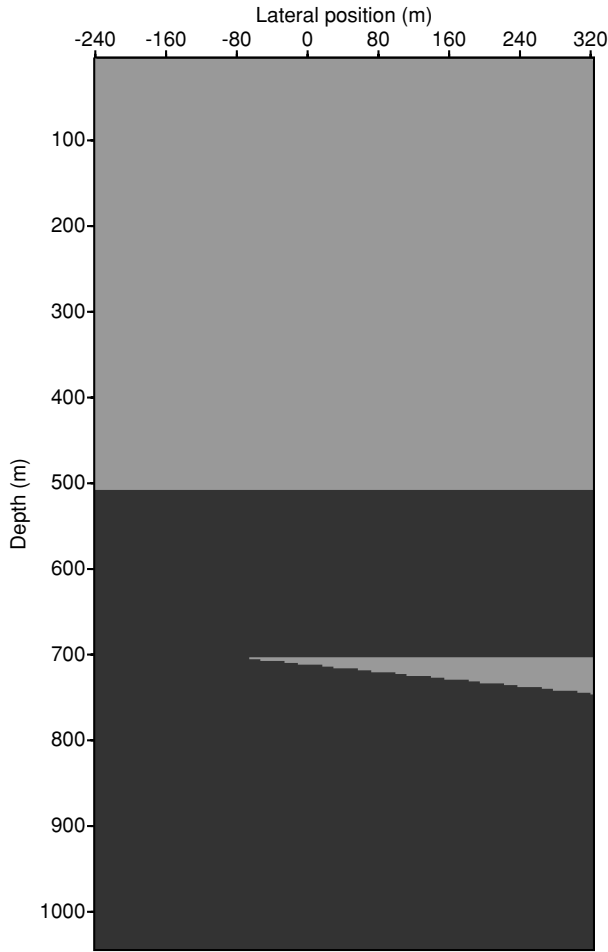


Figure 9 Subsurface velocity model including a sand wedge. The light shading (including the sand) denotes a velocity of 2200 m/s and the dark shading denotes a velocity of 3400 m/s.

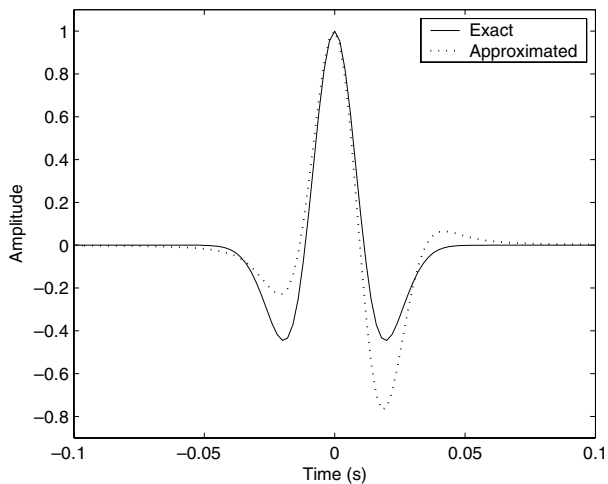


Figure 10 Exact and approximated source wavelets. The synthetic data set is generated using the exact wavelet.

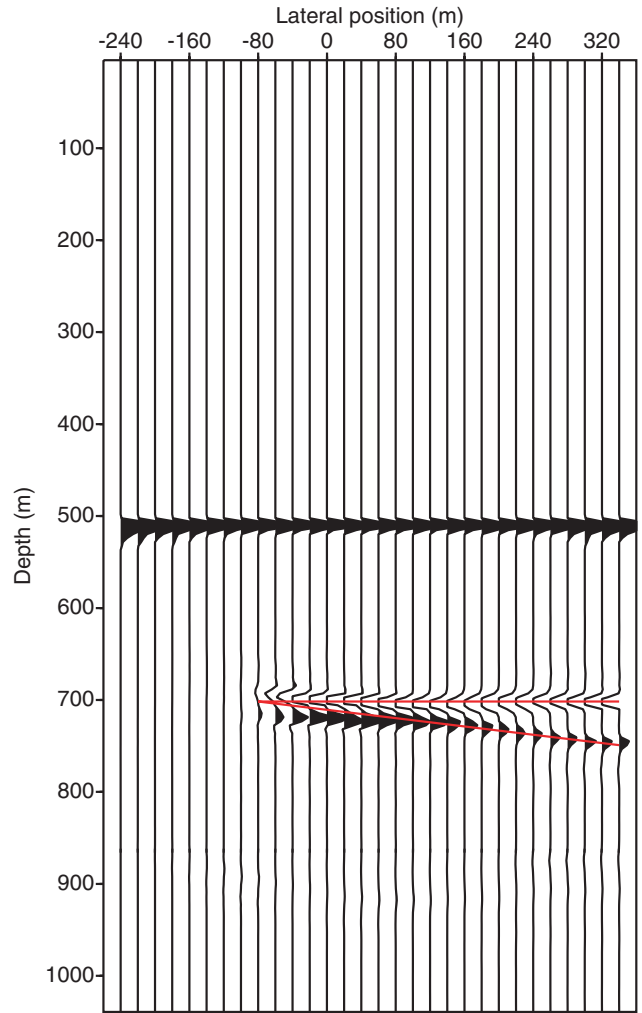
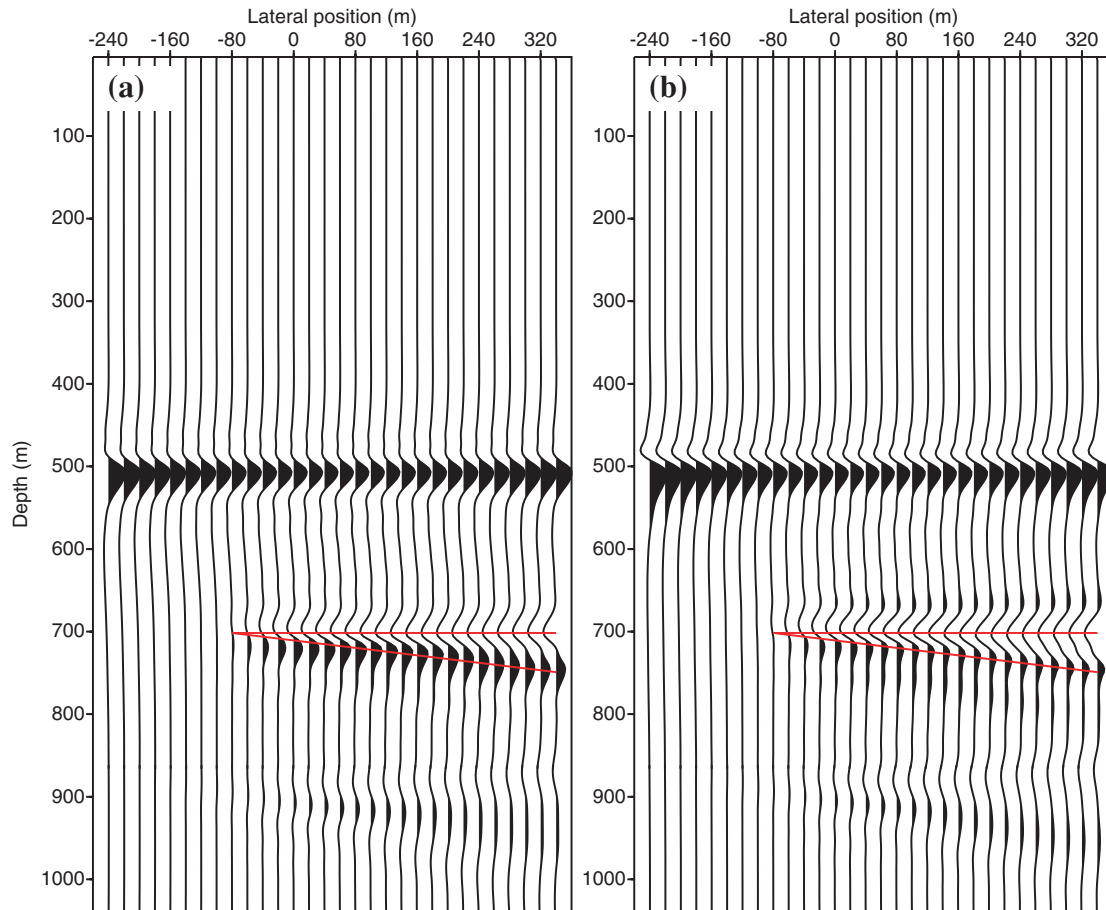


Figure 11 High-resolution imaging obtained by the proposed scheme. In total, 8 shot gathers with shots moving from  $-80$  m to  $200$  m and a shot interval of  $40$  m are applied. The solid-line wedge denotes the interfaces of the sand wedge.

(i.e. direct wave). Figure 5 illustrates the result of the interference, expressed in the frequency domain, where the solid line denotes the interference between the reference arrival and the reflections from the target zone, and the dotted line denotes the amplitude spectrum of the reference arrival, i.e.  $a_1 a_1^*$  in (6). The time-shift can change the result of the interference; therefore, it can serve as an efficient tool for achieving a stabilized solution by changing the cost function in (12) (Zhang 1994).

Figure 6 shows a comparison between the sparse and smoothed solutions obtained using (13). The smoothed solution is obtained from  $\mathbf{W} = \mu \mathbf{I}$  with  $\mu = 0.0005 d_{\max}$ , based on the data shown in Fig. 5. Here,  $d_{\max}$  is the maximum



**Figure 12** Conventional prestack depth-migration results obtained using the same data set as used in Figure 11. (a) The result obtained using the exact wavelet; (b) the result obtained using an approximated wavelet. The solid-line wedge denotes the interfaces of the sand wedge.

modulus among all the diagonal elements of the matrix  $\Gamma^T \Lambda^T \Lambda \Gamma$ . The sparse inversion is solved using a sparseness-constraint matrix  $\mathbf{W}$ , obtained from the smoothed solution using (16) with  $\alpha_{\max} = 2.0$  and  $\alpha_{\min} = 0.0001$ . Figure 6 shows that the sparseness constraint obviously improves the resolution of the resulting reflection coefficients. Comparing Fig. 6 with Figs 2 and 3, we find that the reflections from the closely spaced reflectors are well separated with correct polarity. The internal multiples included in the shot record explain the appearance of small values in the sparse solution.

To assess the robustness of the proposed algorithm under noisy conditions, we add white noise to the reference arrival and reflection data shown in Fig. 4, as illustrated in Fig. 7. Here, the ratio of the rms of the noise to the maximum value of the signal is 0.08 for both the reference arrival and reflection data. The same computational procedure as used to obtain the result in Fig. 6 is applied to the resulting noisy data. The sparse

and smoothed solutions for the noisy data are shown in Fig. 8. Compared with the sparse solution in Fig. 6, we find that a similar sparse solution with the spikes in the same positions is obtained, despite the significant noise in the reference arrival and reflection data. The noise explains the small changes in the magnitudes of the spikes in Fig. 8. This experiment demonstrates the robustness of the proposed algorithm, especially for the positions of the spikes. This result also means that an approximated reference arrival will be sufficient for obtaining high-resolution imaging.

## DEPTH MAPPING

The half-migrated shot gather is expressed in the travelt ime from the source to each spatial gridpoint. Correspondingly, the high-resolution imaging of the reflection coefficients (i.e. reflection series), obtained according to this half-migrated

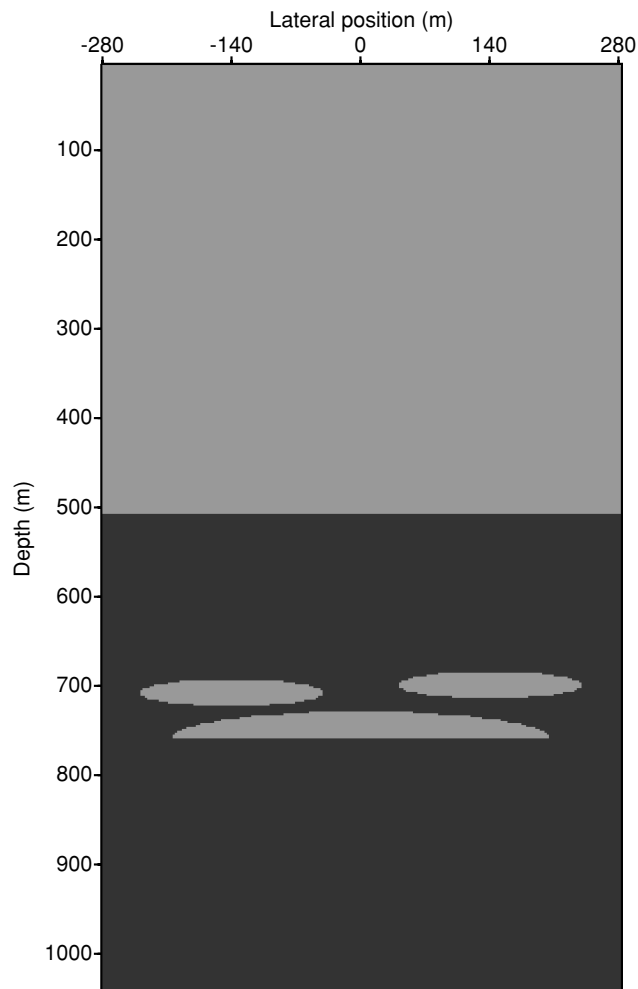


**Figure 13** Subsurface velocity model with several thin sands. The maximum thickness of each of the sands is 30 m. The light shading (including the sands) denotes a velocity of 2200 m/s and the dark shading denotes a velocity of 3400 m/s.

gather by sparse inversion, is also expressed in the same traveltime. Hence, it is necessary to map the resulting high-resolution image from the time domain to the depth domain for common-depth-point stacking. This mapped result represents a high-resolution migrated shot gather. Based on the previously calculated  $T(\mathbf{x})$  in the half-migration process, the depth mapping can be easily accomplished by relating each discretized time point to each depth at each lateral position. Since the peaks are not usually exactly coincident at the same depth points for different migrated shot gathers, due to the approximation in wavefield extrapolation, an interpolation is needed during common-depth-point stacking. The extrapola-

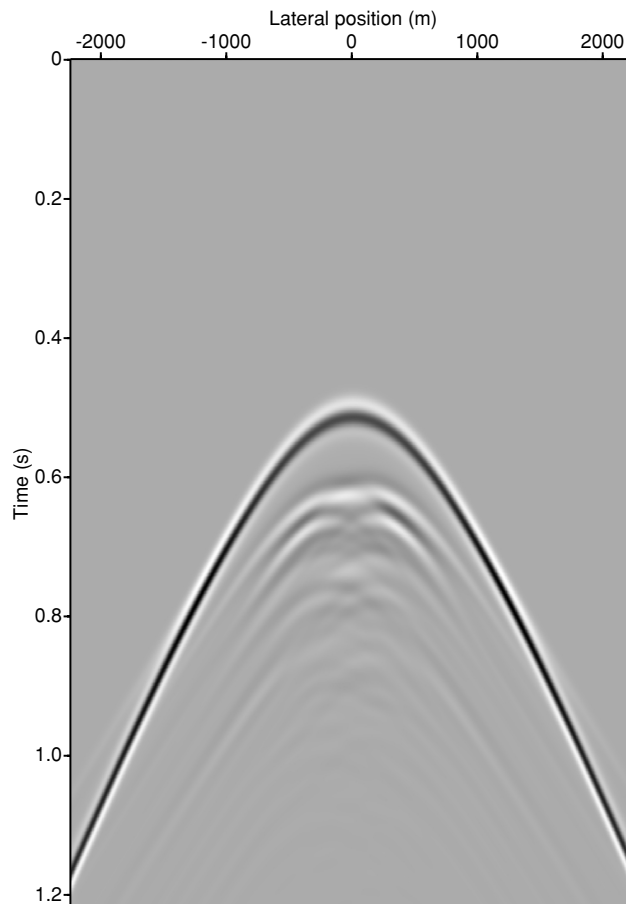


**Figure 14** Shot gather for the source positioned at  $x = 0$ . The shot gather is obtained using an acoustic finite-difference scheme. The direct wave has been removed.

tion and stacking used may slightly degrade the resolution of the resulting imaging but can suppress the noise.

## NUMERICAL EXAMPLES

### Wedge model

A 2D wedge model is now used to evaluate the improvement in the resolution of the proposed imaging technique. The subsurface velocity model is illustrated in Fig. 9, where a flat reflector is well separated from the sand wedge to make it easy to decompose the signal into a reference arrival and a target reflection. The reflection resulting from the flat reflector is taken as the reference arrival. The synthetic data set is generated using an acoustic finite-difference scheme (Zhang 2004) with a wavelet with a peak frequency of 20 Hz, as shown by the solid line in Fig. 10. The high-resolution

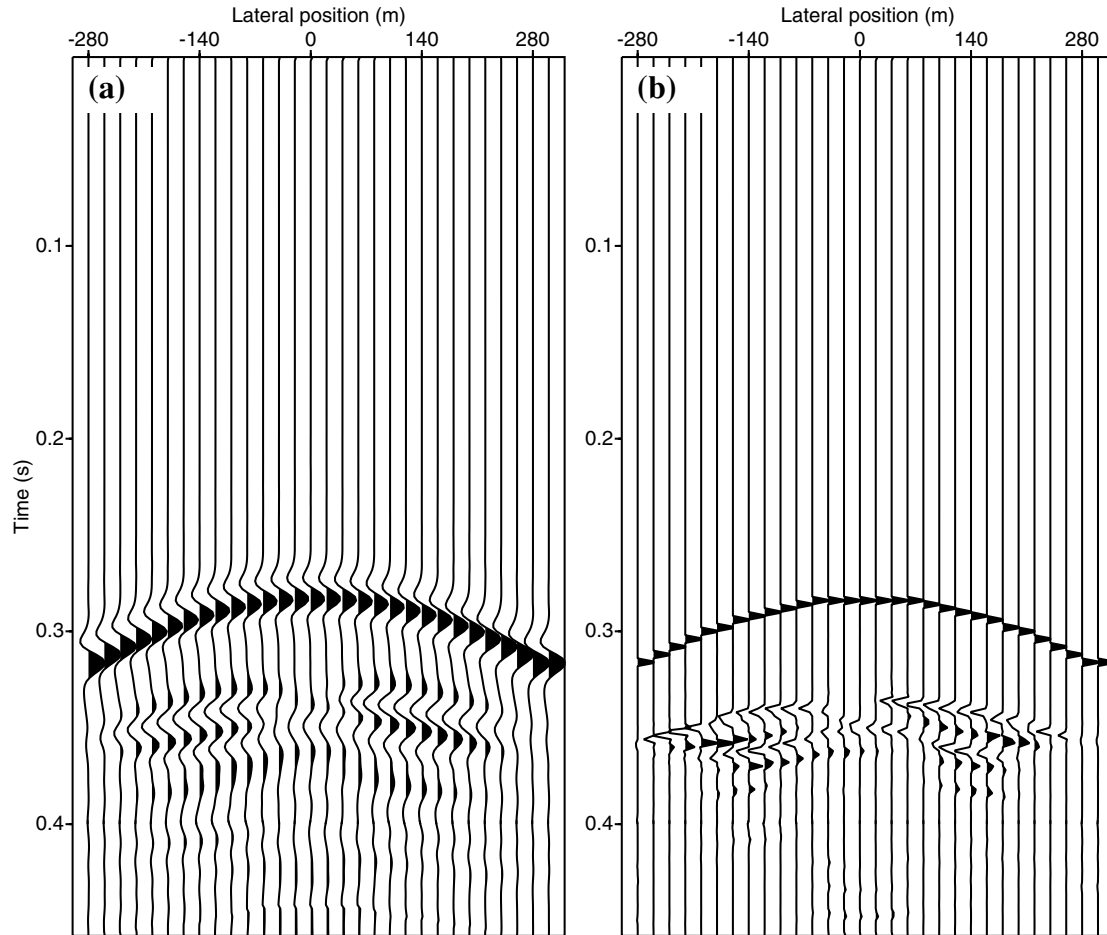


**Figure 15** Half-migrated shot gather (a) and the corresponding high-resolution reflection series (b). (b) is obtained by sparse inversion based on the interferences of the data in (a). The time represents the traveltimes from the source to each depth point at the related lateral position.

imaging obtained by the proposed scheme is shown in Fig. 11, where the solid-line wedge denotes the interfaces of the sand wedge. This high-resolution imaging is a common-depth-point stacked section of eight high-resolution migrated shot gathers with shots moving from  $-80$  m to  $200$  m and a shot interval of  $40$  m. The downward wavefield extrapolation for obtaining the half-migrated shot gathers is carried out using the explicit operator scheme (Zhang *et al.* 2001) with a horizontal spacing of  $20$  m and a vertical step of  $4.33$  m. In contrast, two conventional prestack depth-migration results obtained by the same explicit operator scheme with the same data set are shown in Fig. 12, where (a) is obtained using the exact wavelet (solid line in Fig. 10), and (b) is the result using an approximated wavelet (dotted line in Fig. 10).

It can be observed in Fig. 11 that the effect of the source wavelet is almost fully removed and the resolution is significantly improved. Except for the tip region, the peaks of the

reflection series lie exactly on the interfaces of the sand wedge. The inaccurate position of the peaks of the reflection series in the tip region, as shown in Fig. 11, occurs because the downward wavefield extrapolation cannot account for the small-scale velocity variation in this area in the half-migration processing. Although an exact wavelet is used in Fig. 12(a), only the reflection coefficients with a narrow frequency-band are obtained as would be expected. This leads to a more ambiguous imaging of the interfaces of the sand wedge than in Fig. 11. Figure 12(b) shows poorer imaging in spite of a reasonable estimation of the source wavelet. Moreover, it can be seen, by comparing Fig. 11 with Fig. 12, that the coherent noise originating from the internal multiples is almost fully suppressed by the proposed high-resolution imaging scheme (owing to the sparseness constraint). This experiment demonstrates the significant improvement in the resolution obtained by using the proposed scheme.

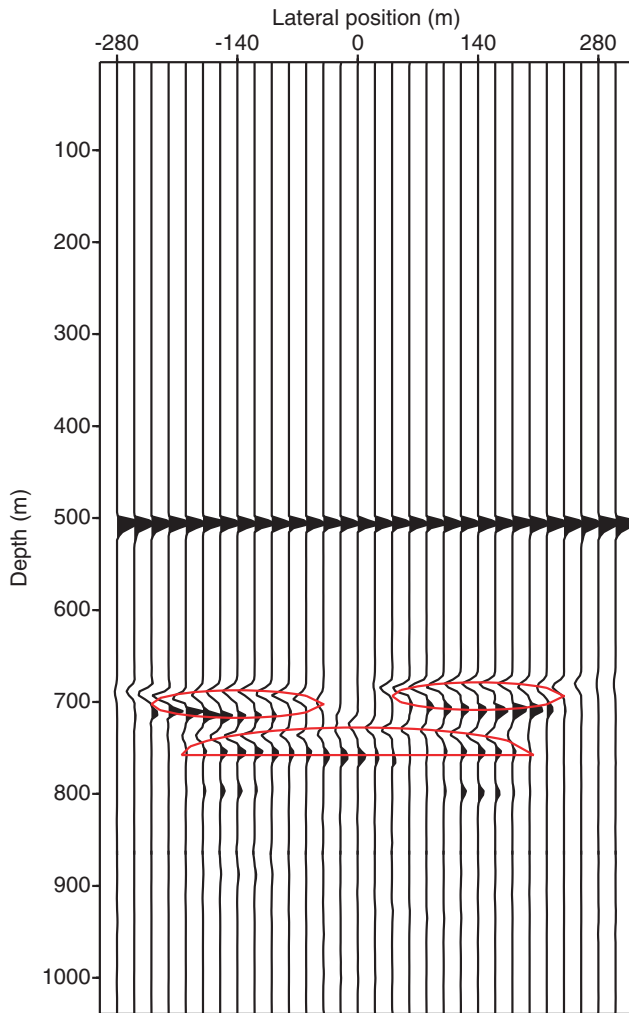


**Figure 16** High-resolution imaging obtained by the proposed scheme. In total, 7 shot gathers with shots moving from  $-120$  m to  $120$  m and a shot interval of  $40$  m are applied. The solid lines denote the interfaces of the three sands.

### Multi-thin-sand model

A slightly more complicated 2D synthetic seismic experiment is designed to test the proposed high-resolution imaging scheme further. The subsurface velocity model is shown in Fig. 13, where the maximum thickness of each of the sands is  $30$  m. Since research on the decomposition of reflection events (performed, for example, by Radon transform or time-frequency spectral analysis) is beyond the scope of this paper, we include a flat reflector well separated from the thin sands, and do not include other curved reflectors in this model. This leads to a simple decomposition and muting processing (i.e. no arrivals need to be muted). Thus, the experiment can fo-

cus on testing the proposed high-resolution imaging scheme. In practice, when the correct decomposition and the corresponding muting processing are employed, it is possible to reduce the realistic structure into an analogue model, as shown in Fig. 13. The reflection resulting from the flat reflector is taken as the reference arrival. In total, seven shot records with shots moving from  $-120$  m to  $120$  m and a shot interval of  $40$  m are generated with an acoustic finite-difference scheme (Zhang 2004). The wavelet used is the same as that used in the foregoing example, i.e. the solid line shown in Fig. 10, with a peak frequency of  $20$  Hz. Thus, the dominant wavelength of the seismic signals is  $110$  m in the relevant sands and  $170$  m in the background medium. A typical shot gather for the source positioned at  $x = 0$  is shown in Fig. 14, where the direct wave has been removed. A horizontal spacing of  $20$  m and a vertical step of  $4.33$  m are used in the half-migration processing.

A half-migrated shot gather and the corresponding high-resolution reflection series are shown in Fig. 15 for the source positioned at  $x = 0$ . The explicit operator scheme (Zhang *et al.* 2001) is used in the half-migration process, and the values  $\mu = 0.006d_{\max}$ ,  $\alpha_{\max} = 100.0$  and  $\alpha_{\min} = 0.006$  are used to obtain the smoothed and sparse solutions. The common-depth-point stacked section of a total of seven high-resolution migrated shot gathers is shown in Fig. 16, where the solid lines denote the three thin sands. In this figure, we see that the effect of the source wavelet is almost fully removed and the resolution is significantly improved. It can also be seen that the peaks of the reflection series lie exactly on the interfaces of the thin sands with correct polarity. The internal multiples included in the shot records explain the fact that the reflection coefficients at parts of the reflectors are a little lower in Fig. 16.

In contrast, two conventional prestack depth migration results obtained by the same explicit operator scheme with the same data set are shown in Fig. 17, where (a) is obtained using the exact wavelet (solid line in Fig. 10), and (b) is the result using an approximated wavelet (dotted line in Fig. 10). The flat bottom of the lowest sand is ambiguous in Fig. 17, whereas a flat reflector is visible in Fig. 16. Also, the separations of the sands are clearer in Fig. 16 than in Fig. 17. Compared with the high-resolution imaging of Fig. 16, the shapes of the sands are inaccurate in Fig. 17(a) despite the fact that an exact wavelet is used, and they are even poorer in Fig. 17(b), although a reasonable estimated wavelet is used. Comparing Fig. 16 with Fig. 17, we also see that the proposed high-resolution imaging scheme efficiently suppresses the coherent noise originating from the internal multiples. These comparisons demonstrate the quality of the proposed scheme. This experiment shows

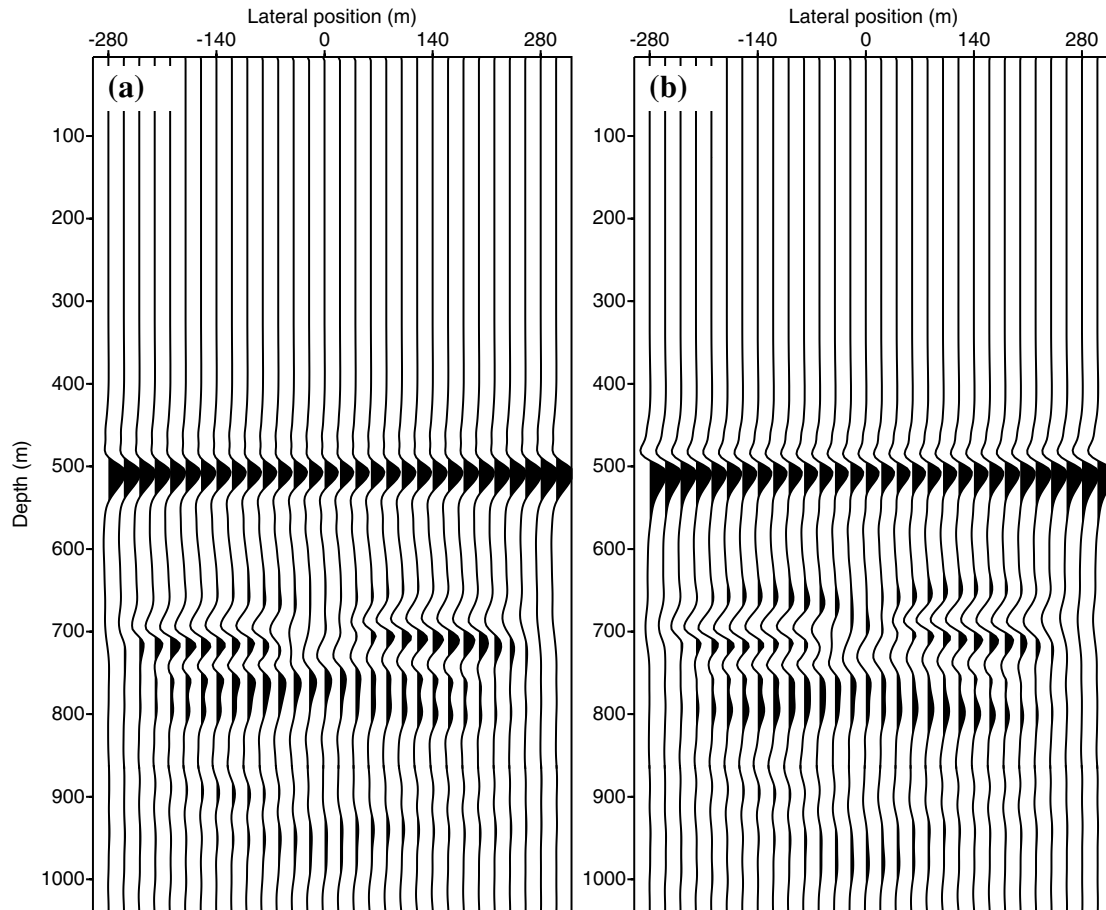


Figure 17 Conventional prestack depth-migration results obtained using the same data set as used in Figure 16. (a) is the result obtained using the exact wavelet, and (b) is obtained using an approximated wavelet.

that it is possible to use the proposed scheme to image stacked sheet sand structures.

## CONCLUSIONS

An imaging technique for improving the resolution of thin layers has been presented. An interference technique is proposed, which replaces the imaging process of depth migration by a least-squares inversion, and a proposed sparse constraint is introduced for improving the resolution of the resulting imaging. The proposed scheme needs to be used after application of a decomposition algorithm, e.g. a Radon transform or time-frequency spectral analysis, which helps to obtain a decomposed signal or combined event and to mute reflections resulting from reflectors other than the target zone of interest. In contrast to conventional depth imaging schemes, a reference arrival, instead of a source wavelet, is required, and in con-

trast to current sparse-spike inversion techniques, a decomposition algorithm, instead of the appraisal deconvolution, has to be applied in advance. The proposed scheme should be used following conventional depth imaging if higher resolution is needed in a target zone, rather than replacing the conventional imaging schemes for the entire medium.

The good performance of the proposed sparse inversion algorithm has been demonstrated by a computed point-source response from a model with two closely spaced thin layers under noise-free as well as noisy conditions. Synthetic data sets, obtained by an acoustic finite-difference method, were used to test the proposed imaging scheme. The numerical examples show a significant improvement in resolution when imaging is carried out with the proposed high-resolution scheme, compared with the imaging obtained by conventional prestack depth-migration schemes using either an exact or an approximated source wavelet.

## ACKNOWLEDGEMENTS

J. Z. thanks the Netherlands Research Centre for Integrated Solid Earth Science for supporting his research fellowship at Delft University of Technology.

## REFERENCES

- Berkhout A.J. 1982. Seismic Migration, Imaging of Acoustic Energy by Wave Field Extrapolation, A: *Theoretical Aspects*. Elsevier. Science Publishing Co.
- Buske S. and Kastner U. 2004. Efficient and accurate computation of seismic traveltimes and amplitudes. *Geophysical Prospecting* **52**, 313–322.
- Claerbout J.F. 1971. Toward a unified theory of reflector mapping. *Geophysics* **36**, 467–481.
- Claerbout J.F. 1976. *Fundamentals of Geophysical Data Processing*. McGraw–Hill Book Co.
- Hu J., Schuster G.T. and Valasek P.A. 2001. Poststack migration deconvolution. *Geophysics* **66**, 939–952.
- Jin S., Madariaga R., Virieux J. and Lambaré G. 1992. Two dimensional asymptotic iterative elastic inversion. *Geophysical Journal International* **108**, 575–588.
- Levy S. and Fullagar P.K. 1981. Reconstruction of a sparse spike train from a portion of its spectrum and application to high-resolution deconvolution. *Geophysics* **46**, 1235–1243.
- Oldenburg D.W., Scheuer T. and Levy S. 1983. Recovery of the acoustic impedance from reflection seismograms. *Geophysics* **48**, 1318–1337.
- Pinnegar C.R. and Mansinha L. 2003. The S-transform with windows of arbitrary and varying shape. *Geophysics* **68**, 381–385.
- Robinson E. 1967. Predictive decomposition of time series with application to seismic exploration. *Geophysics* **32**, 418–484.
- Sacchi M.D. and Ulrych T.J. 1996. Estimation of the discrete Fourier transform— A linear inversion approach. *Geophysics* **61**, 1128–1136.
- Sacchi M.D., Velis D.R. and Cominquez A.H. 1994. Minimum entropy deconvolution with frequency domain constraints. *Geophysics* **59**, 938–945.
- Trad D., Ulrych T. and Sacchi M. 2003. Latest views of the sparse Radon transform. *Geophysics* **68**, 386–399.
- Walker C. and Ulrych T.J. 1983. Autoregressive recovery of acoustic impedance. *Geophysics* **48**, 1338–1350.
- Wang Y. 2003. Sparseness-constrained least-square inversion: Application to seismic wave reconstruction. *Geophysics* **68**, 1633–1638.
- Welford W.T. 1981. *Optics*. Oxford University Press.
- Zhang J. 1994. A convergent iterative algorithm for solving elastic waveform inversion. *Science in China (Series a)* **37**, 459–468.
- Zhang J. 2004. Wave propagation across fluid–solid interfaces: a grid method approach. *Geophysical Journal International* **159**, 240–252.
- Zhang J., Verschuur D.J. and Wapenaar C.P.A. 2001. Depth migration of shot records in heterogeneous, transversely isotropic media using optimum explicit operators. *Geophysical Prospecting* **49**, 287–299.